





RESEARCH ARTICLE | JULY 15 2025

Giant magnetocaloric effect of divalent europium-based oxide composites of Eu_2TiO_4 and $\text{Eu}_3\text{Ti}_2\text{O}_7$ for cryogenic temperature magnetic refrigeration

Koichi Matsumoto ; Masaki Horie; Hironori Hasegawa; Kazuhiro Ishikawa; Shuhei Yamazaki; Hideaki Kitazawa ; Akiko T. Saito ; Takenori Numazawa 



J. Appl. Phys. 138, 033901 (2025)

<https://doi.org/10.1063/5.0278479>



Articles You May Be Interested In

Large reversible magnetocaloric effect in TmTiO_3 single crystal

J. Appl. Phys. (March 2012)

Octahedral tilt independent magnetism in confined GdTiO_3 films

Appl. Phys. Lett. (March 2018)

Structural, magnetic, and electronic properties of GdTiO_3 Mott insulator thin films grown by pulsed laser deposition

Appl. Phys. Lett. (October 2014)



Nanotechnology & Materials Science



Optics & Photonics



Impedance Analysis



Scanning Probe Microscopy



Sensors



Failure Analysis & Semiconductors



Unlock the Full Spectrum.
From DC to 8.5 GHz.

Your Application. Measured.

Find out more



Giant magnetocaloric effect of divalent europium-based oxide composites of Eu_2TiO_4 and $\text{Eu}_3\text{Ti}_2\text{O}_7$ for cryogenic temperature magnetic refrigeration

Cite as: J. Appl. Phys. 138, 033901 (2025); doi: 10.1063/5.0278479

Submitted: 30 April 2025 · Accepted: 24 June 2025 ·

Published Online: 15 July 2025



Koichi Matsumoto,^{1,a)} Masaki Horie,¹ Hironori Hasegawa,¹ Kazuhiro Ishikawa,² Shuhei Yamazaki,² Hideaki Kitazawa,³ Akiko T. Saito,³ and Takenori Numazawa³

AFFILIATIONS

¹Department of Physics, Kanazawa University, Kakuma-machi, Kanazawa 920-1192, Japan

²Corporate Fine Ceramics Group, Kyocera Corporation, Kyoto-shi, Kyoto 612-8501, Japan

³National Institute for Materials Science (NIMS), Tsukuba 305-0003, Japan

^{a)}Author to whom correspondence should be addressed: k.matsu@staff.kanazawa-u.ac.jp

ABSTRACT

For cryogenic temperature magnetic refrigeration, we focused on materials containing Eu^{2+} ions and synthesized sintered composite materials comprising Eu_2TiO_4 and $\text{Eu}_3\text{Ti}_2\text{O}_7$. $\text{Eu}_3\text{Ti}_2\text{O}_7$ and Eu_2TiO_4 exhibited second-order phase transitions between the paramagnetic and ferromagnetic states at 7 and 8 K, respectively. The magnetocaloric effect was evaluated from magnetization and specific heat. It was shown that Eu^{2+} ions behave similarly to free ions with $J = 7/2$. The maximum magnetic entropy change per unit volume exceeded $0.3 \text{ J/cm}^3\text{K}$ at a magnetic field of 5 T. The Carnot cycle at the hydrogen liquefaction temperature was evaluated using the obtained entropy temperature diagram. It was found that the cooling capacity is several times higher than that of known materials such as $\text{Gd}_3\text{Ga}_5\text{O}_{12}$, $(\text{Dy}_{0.8}\text{Gd}_{0.2})_3\text{Al}_5\text{O}_{12}$, and GdTlO_3 . It was also shown that the present composite materials are useful for extending the operating temperature range of the adiabatic demagnetization refrigerator. These results indicate that Eu_2TiO_4 and $\text{Eu}_3\text{Ti}_2\text{O}_7$ composites are promising magnetic refrigerants for cryogenic magnetic refrigeration.

© 2025 Author(s). All article content, except where otherwise noted, is licensed under a Creative Commons Attribution-NonCommercial-NoDerivs 4.0 International (CC BY-NC-ND) license (<https://creativecommons.org/licenses/by-nc-nd/4.0/>). <https://doi.org/10.1063/5.0278479>

I. INTRODUCTION

Magnetic refrigeration has emerged as a leading candidate to replace conventional gas expansion refrigerators. This approach utilizes the magnetocaloric effect (MCE), a phenomenon in which a change in an externally applied magnetic field causes a corresponding temperature variation in a magnetic material (the refrigerant). The concept of utilizing the MCE for solid-state cooling was initially proposed by Debye¹ and Giauque.² Since that time, the field has undergone substantial advancements. The potential benefits of high efficiency, reduced environmental impact, compact size, and silent operation have prompted substantial research in novel magnetic materials and refrigeration system architectures, spanning a wide temperature range.^{3–6}

Hydrogen, a clean and environmentally benign energy carrier, offers a promising solution to growing energy demands. The

utilization of this technology serves to mitigate the release of greenhouse gases and pollutants into the atmosphere. Liquid hydrogen, characterized by its high density, is considered an optimal medium for storage and transportation.^{7,8} Although Joule–Thomson expansion remains the prevailing standard for hydrogen liquefaction, magnetic cooling has garnered considerable attention due to its ability to improve energy efficiency.

Significant advancements in the field of hydrogen liquefaction have been achieved through the development of magnetic refrigeration technology. Numazawa *et al.*,^{9,10} Matsumoto *et al.*,¹¹ and Ohira *et al.*¹² have demonstrated successful hydrogen liquefaction using the Carnot cycle. In the recent study, Kamiya *et al.*¹³ reported the successful implementation of liquefaction using an active magnetic regenerator (AMR) cycle.

In the liquefaction stage, the Carnot magnetic refrigerator (CMR) was utilized, employing a heat pipe to condense the

hydrogen gas directly on the surface of the magnetic material. This method has been demonstrated to achieve significantly higher thermal efficiency in comparison with the conventional approach that utilizes the Joule–Thomson valve. The magnetic refrigerant employed in this CMR design must exhibit a substantial magnetocaloric effect (MCE) coupled with robust chemical stability against hydrogenation. To meet these criteria, Ohira used a single crystal gadolinium gallium garnet, $\text{Gd}_3\text{Ga}_5\text{O}_{12}$ (GGG)¹² and our group selected a ceramic Dy-substituted gadolinium aluminum garnet, $(\text{Dy}_{0.8}\text{Gd}_{0.2})_3\text{Al}_5\text{O}_{12}$ (DGAG)⁹ as the magnetic refrigerant.

The operation of astronomical instruments, such as the transition edge sensor (TES), requires cooling methods that can attain sub-Kelvin temperatures to ensure optimal sensitivity. In order to facilitate continuous cooling at these temperatures, the cryogenic group at NASA's Goddard Space Flight Center (GSFC) has developed a multi-stage continuous adiabatic demagnetization refrigerator (ADR).^{14,15} The capabilities of the technology have been demonstrated by a four-stage cascaded ADR (CADR) operating between 50 mK and 4.5 K. In the higher temperature stages of these ADRs, GGG is typically employed as the magnetic refrigerant. Gadolinium lithium fluoride (GdLiF_4 , GLF) has also been explored as a potential alternative in these stages because of its attractive magnetic characteristics.^{16,17}

Numerous magnetic materials have been investigated as potential refrigerants for cryogenic temperatures.^{3–6,18,19} The selection of appropriate materials that have large magnetic entropy change (ΔS_m) and proper transition temperature (T_c) is crucial for magnetic refrigeration.

Gadolinium (Gd^{3+}) ions are of interest due to their substantial magnetic moment ($J = 7/2$). The absence of spin–orbit coupling in Gd^{3+} generally leads to highly degenerated localized magnetic moments within the crystal lattice, allowing these moments to be maintained even at low temperatures.²⁰ GGG is used as a standard magnetic refrigerant in cryogenic temperatures.^{19,21–24} A series of Fe-modified gadolinium gallium garnets ($\text{Gd}_3(\text{Ga}_{1-x}\text{Fe}_x)_5\text{O}_{12}$, GGIG) was demonstrated to exhibit a larger ΔS_m than that of GGG at 20 K.^{25,26} Polycrystalline plates and spheres composed of GGG, DGAG, and GGIG were synthesized and examined in magnetic refrigerators.^{10,11,19}

Furthermore, the MCE has been extensively studied in perovskite oxides such as GdTiO_3 (GTP),²⁷ GdAlO_3 (GAP),^{28,29} DyTiO_3 ,³⁰ HoTiO_3 ,³¹ TmTiO_3 ,³² and EuTiO_3 (ETP).^{33,34}

In this study, we investigated the potential of divalent europium (Eu^{2+}) compounds as magnetic refrigerants. The $4f^7$ electron configuration ($J = 7/2$) of Eu^{2+} ions has been shown to minimize crystalline electric field effects and magnetic anisotropy, thereby promoting a large and isotropic MCE. The ferromagnetic chalcogenides EuO ($T_c = 69$ K)³⁵ and EuS ($T_c = 18$ K), both with NaCl structures, have been previously studied for their substantial MCE.^{36–38}

In the ternary Eu–Ti–O system, McCarthy *et al.* identified several compounds.³⁹ ETP, a multiferroic with a cubic perovskite structure ($a = 3.90$ Å) exhibits G-type antiferromagnetic ordering at 5.5 K, and its magnetic properties have been studied.^{40–43} The large MCE has also been reported.³⁴

Eu_2TiO_4 and $\text{Eu}_3\text{Ti}_2\text{O}_7$ are distinguished by their layered perovskite structures, which are characteristic of the Ruddlesden–

Popper phases. The general formula for these phases is written as $A_{n-1}A'B_nX_{3n+1}$, where A , A' , and B represent cations, X is an anion, and n designates the number of octahedral layers in the perovskite-like stack. The crystal structure of Eu_2TiO_4 ($n = 1$) exhibits a K_2NiF_4 -type structure (space group $I4/mmm$) with a tetragonal unit cell ($a = 3.883$ Å and $c = 12.523$ Å) containing two formula units. That of $\text{Eu}_3\text{Ti}_2\text{O}_7$ ($n = 2$) also exhibits a tetragonal structure (space group $I4/mmm$, $a = 3.90$ Å, $c = 20.28$ Å) and consists of alternating layers of EuTiO_3 and Eu_2TiO_4 , with two non-equivalent Eu sites. The number of Eu_2TiO_4 sites is twice that of EuTiO_3 sites.^{44,45} The crystal structures of Eu_2TiO_4 and $\text{Eu}_3\text{Ti}_2\text{O}_7$ are depicted in Fig. 1.

Magnetization (M) studies of ETP, Eu_2TiO_4 , and $\text{Eu}_3\text{Ti}_2\text{O}_7$ have been conducted.⁴⁶ Eu_2TiO_4 and $\text{Eu}_3\text{Ti}_2\text{O}_7$ were found to be ferromagnetic with T_c of 9 and 8.5 K, respectively. In addition, ^{151}Eu Mössbauer spectroscopy further revealed Eu_2TiO_4 to be ferromagnets with a T_c of 7.8 K, suggesting a ferrimagnetic ordering due to positive exchange interaction between inequivalent EuTiO_3 and Eu_2TiO_4 sublattices.^{40,47}

Eu_2TiO_4 and $\text{Eu}_3\text{Ti}_2\text{O}_7$ were identified as promising magnetic refrigerants for cryogenic applications due to their suitable transition temperatures and ferromagnetic interactions. Consequently, composite ceramic materials comprising Eu_2TiO_4 and $\text{Eu}_3\text{Ti}_2\text{O}_7$ were synthesized. The MCE of these composites, as evaluated from M and specific heat (C) measurements, exhibits a substantial increase compared to that of other oxide materials. Furthermore, the volumetric cooling capacity of our composites in a Carnot cycle for hydrogen liquefaction was found to be several times larger than that of GGG and DGAG. These materials also exhibit potential for extending the operating temperature range of ADRs to higher temperatures.

II. EXPERIMENTAL PROCEDURE

The synthesis of ceramic composite materials was conducted as follows: Eu_2O_3 and TiO powders were weighed out in several ratios near 1:1. Subsequently, the raw powders were meticulously milled in isopropyl alcohol using a ball mill. Subsequent to milling, an organic binder was incorporated into the mixture, and the mixture was granulated while volatilizing the isopropyl alcohol. The granulated mixture was subsequently pressurized and molded at 147 MPa to yield disk-shaped pellets with a diameter of 12 mm and a thickness of 3 mm. The preparation of the ceramic samples was conducted with the heating of the pellets at two distinct temperatures: 1400 °C for samples 1 and 3 and 1500 °C for sample 2. Samples for magnetization and specific heat measurements were cut from these sintered pellets.

Due to difficulties in acquiring a single-phase material, the decision was made to synthesize composite samples. Three distinct compositions were prepared: sample 1, composed of $\text{Eu}_3\text{Ti}_2\text{O}_7$ and Eu_2O_3 ; sample 2, composed of Eu_2TiO_4 and $\text{Eu}_3\text{Ti}_2\text{O}_7$; and sample 3, composed of Eu_2TiO_4 , $\text{Eu}_3\text{Ti}_2\text{O}_7$, and Eu_2O_3 . As illustrated in Fig. 1, the powder XRD pattern of sample 3 reveals the presence of three crystalline phases. As shown in Table I, the composition ratios for each sample are determined by means of Rietveld refinement.

18 August 2025 09:55:45

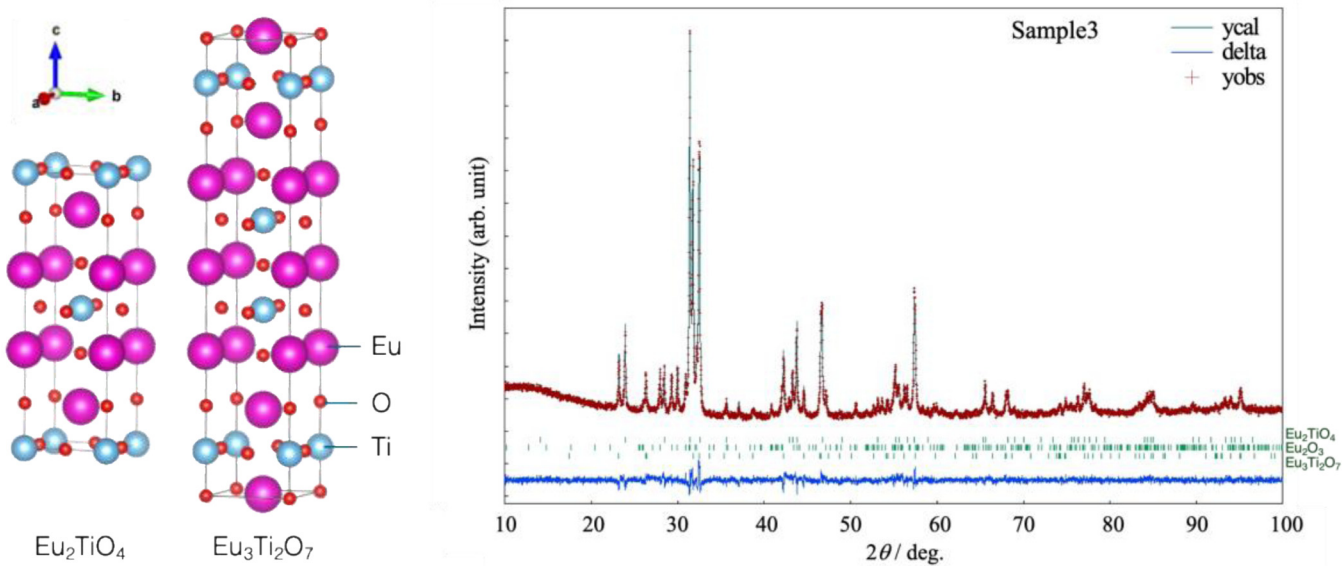


FIG. 1. (Left) crystal structures of Eu_2TiO_4 and $\text{Eu}_3\text{Ti}_2\text{O}_7$ drawn using VESTA.⁴⁸ (Right) x-ray powder diffraction pattern of the composite (sample 3). Vertical bars represent diffraction angles of Eu_2TiO_4 , $\text{Eu}_3\text{Ti}_2\text{O}_7$, and Eu_2O_3 .

The synthesis of high-density sintered pellets with low porosity was successfully achieved. The bulk densities of the sintered samples were determined using Archimedes' principle. The measured bulk densities are also presented in Table I.

The temperature dependences of magnetization (M - T) were measured using a Quantum Design SQUID magnetometer MPMS in applied magnetic fields ranging from 0.1 to 5 T. Rectangular rod-shaped samples with dimensions of $0.55 \times 0.55 \times 3.30 \text{ mm}^3$ were used for these measurements. The magnetic field was applied along the longitudinal direction of the rods to minimize demagnetization effects.

Specific heat measurements were conducted using a thermal relaxation method with a Quantum Design PPMS. Plate-shaped samples with dimensions of $2.0 \times 2.0 \times 1.1 \text{ mm}^3$ were used for the measurements in the temperature range of 2–300 K.

III. RESULTS

A. Specific heat and entropy

Figure 2 shows the temperature dependence of C for three samples in the zero magnetic field. The sharpness of these peaks

indicates the high quality of the synthesized materials. In Eu_2O_3 , europium exists as Eu^{3+} ion, which has a significantly smaller magnetic moment compared to the Eu^{2+} ion. Consequently, the magnetic specific heat of Eu_2O_3 is considered negligible, and its total heat capacity is primarily attributed to the lattice contribution.^{49,50} Sample 1 is mainly composed of $\text{Eu}_3\text{Ti}_2\text{O}_7$, so the specific heat peak at 7 K is attributed to $\text{Eu}_3\text{Ti}_2\text{O}_7$. Two different peaks are

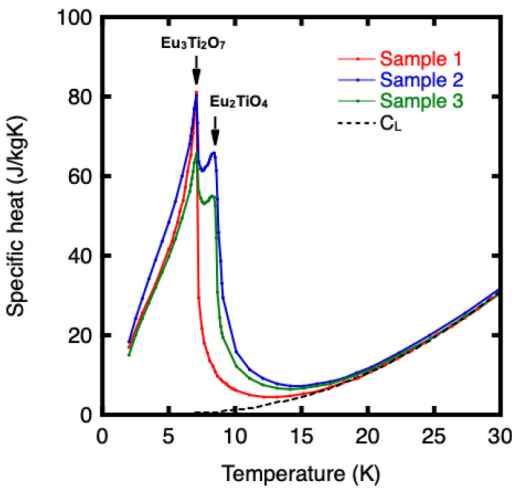


FIG. 2. Temperature dependence of specific heat for samples 1, 2, and 3 in the zero magnetic field. The dashed line shows the lattice specific heat C_L obtained from a Debye model fit.

TABLE I. Composition ratios of Eu_2TiO_4 , $\text{Eu}_3\text{Ti}_2\text{O}_7$, and Eu_2O_3 constituting samples 1, 2, and 3. Bulk density is also shown for each sample.

Sample	Eu_2TiO_4 (wt. %)	$\text{Eu}_3\text{Ti}_2\text{O}_7$ (wt. %)	Eu_2O_3 (wt. %)	Bulk density (g/cm ³)
1	0.0	80.0	20.0	7.05
2	56.2	43.8	0.0	6.99
3	44.4	37.6	18.0	7.01

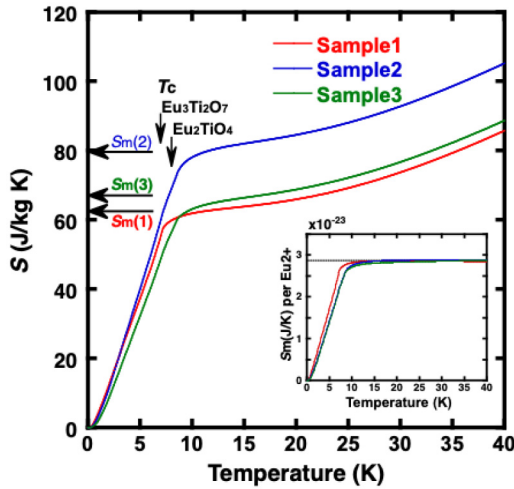


FIG. 3. Temperature dependence of entropy for samples 1, 2, and 3 in the zero magnetic field. Horizontal arrows indicate the theoretical S_m caused by Eu_2TiO_4 and $\text{Eu}_3\text{Ti}_2\text{O}_7$ for each sample. Vertical arrows indicate T_c of Eu_2TiO_4 and $\text{Eu}_3\text{Ti}_2\text{O}_7$. The inset shows magnetic entropy S_m per Eu^{2+} ion for each sample. The dashed line in the inset represents the theoretical S_m for a free ion with $J = 7/2$ (see text for details).

observed in samples 2 and 3, which have $\text{Eu}_3\text{Ti}_2\text{O}_7$ and Eu_2TiO_4 . Therefore, we consider that the specific heat peak at 8 K is attributed to Eu_2TiO_4 . The transition temperatures attributed to $\text{Eu}_3\text{Ti}_2\text{O}_7$ and Eu_2TiO_4 are both lower relative to those in the literature,⁴⁶ respectively, but the high-low relation of the T_c is the same. Therefore, the specific heat peaks at 7 and 8 K are identified as those of $\text{Eu}_3\text{Ti}_2\text{O}_7$ and Eu_2TiO_4 , respectively. The slight difference in the T_c values from the literature may be due to sample dependence on oxygen deficiency or other factors. The relative magnitudes of the peaks are qualitatively consistent with the compositional ratios of the samples. Above 20 K, the C of each sample increases with temperature and converges, indicating that the lattice heat capacity becomes the dominant contribution in this temperature range.

The total entropy (S) was calculated by integrating C/T with respect to temperature in a constant magnetic field (H) as

$$\Delta S(T, H) = \int_0^T \left(\frac{C}{T} \right)_H dT. \quad (1)$$

Figure 3 presents the S of all the samples in the zero field calculated using Eq. (1). The C data below 2 K were smoothly extrapolated to 0 at absolute zero before integration. A clear release of magnetic entropy (S_m) is observed below 10 K for each sample. As discussed earlier, the increase in S above 20 K is attributed to the lattice contribution. The total S appears to correlate with the amount of Eu_2TiO_4 and $\text{Eu}_3\text{Ti}_2\text{O}_7$ in each sample. The total amount of Eu^{2+} ions ($N_{\text{Eu}^{2+}}$) was determined from the composition ratio in Table I, yielding values of $3.62 \times N_A$, $4.68 \times N_A$, and $3.84 \times N_A$ (N_A , the Avogadro constant) per kilogram for samples 1,

2, and 3, respectively. The theoretical magnetic entropy S_m for 1 mol of ions with spin J is given by $R \ln(2J + 1)$, where R is the ideal gas constant. Then, this theoretical value for each sample ($N_{\text{Eu}^{2+}} \times R \ln(2J + 1)$) is indicated as a horizontal arrow in Fig. 3 for each sample. The measured S_m values are in good quantitative agreement with these theoretical predictions.

In order to isolate the magnetic contribution of the Eu^{2+} ion to the total S , we fitted C above 20 K using the Debye model. This allowed us to extract the lattice specific heat (C_L) and subsequently determine the magnetic specific heat. The inset in Fig. 3 shows the temperature dependence of S_m per Eu^{2+} ion. The dashed line represents the theoretical value of $k_B \ln(2J + 1)$ for a free ion with $J = 7/2$, where k_B is Boltzmann's constant. The Eu^{2+} ions release almost 100% of their theoretical magnetic entropy during the magnetic transition for each sample. The ionic valence of the Ti atom is inferred to be in the tetravalent state, which has less contribution to magnetic ordering.

B. Magnetization and entropy change

Figure 4 shows the temperature dependence of M for samples 1, 2, and 3, respectively, in applied magnetic fields up to 5 T. In each constant field, the M increases rapidly around 10 K with decreasing temperature. Higher M values were observed for samples with the lower Eu_2O_3 content. However, while two distinct peaks were observed in the C data in Fig. 2, the two corresponding ferromagnetic transitions of Eu_2TiO_4 and $\text{Eu}_3\text{Ti}_2\text{O}_7$ are not clearly observed in the M - T curves. No stepwise increase in M was observed. This is probably due to the smooth increase in M characteristic of the second order phase transition, coupled with the close proximity of the two T_c . A comparison of the temperature derivative of the magnetization ($\frac{\partial M}{\partial T}$) at 0.1 T shown in Fig. 5 reveals a single dip for each sample, with the dip temperature varying according to the composition ratio. The magnetic moment of Eu_2O_3 is considered negligible compared to that of Eu_2TiO_4 and $\text{Eu}_3\text{Ti}_2\text{O}_7$.^{49,50}

Figure 6 shows the inverse magnetic susceptibilities of our composite samples at 0.1 T. Above T_c , the inverse susceptibilities increase linearly with increasing temperature, consistent with the Curie-Weiss behavior. Then, using a rough approximation that assumes two close phase transitions as a single transition, we applied a Curie-Weiss fit to this high temperature region to estimate the effective magnetic moment per Eu^{2+} ion and the paramagnetic Curie temperature. The obtained effective magnetic moments per Eu^{2+} ion were 7.8, 7.9, and $8.0 \mu_B$ (Bohr magneton) for samples 1, 2, and 3, respectively. The corresponding paramagnetic Curie temperatures were 7.6, 9.2, and 8.6 K. These effective magnetic moments are in reasonable agreement with the theoretical value of $7.9 \mu_B$ expected for a $J = 7/2$ spin state. This agreement further supports the conclusion that the Eu^{2+} ion has a $J = 7/2$ magnetic moment and the ionic valence of the Ti atom is in the tetravalent state, which has no magnetic moment under this rough assumption.

At low temperatures and high magnetic fields, M tends to saturate. The saturation magnetization for an ion with spin J is given by $g \mu_B J$, where g is the Landé g -factor. The electron configuration of Eu^{2+} ion results in $g = 2$. Assuming that the saturation

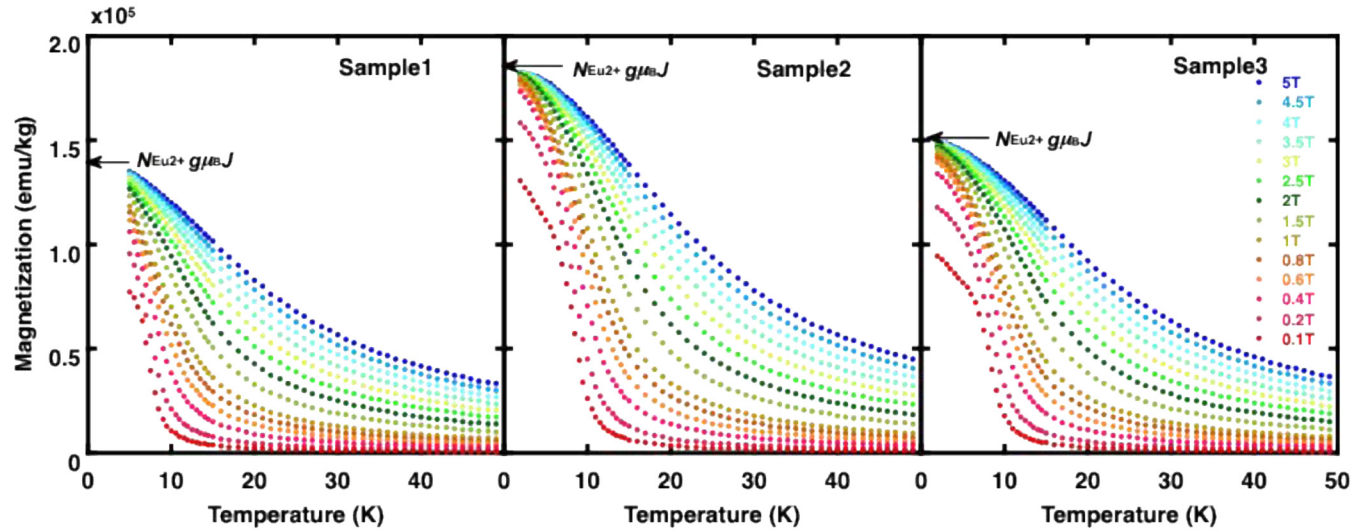


FIG. 4. Temperature dependence of the magnetization in applied fields of 0.1, 0.2, 0.4, 0.6, 0.8, 1, 1.5, 2, 2.5, 3, 3.5, 4, 4.5, and 5 T. Arrows indicate the calculated saturation magnetization for Eu^{2+} free ions (see text for details).

magnetization is primarily due to the Eu^{2+} ions present in Eu_2TiO_4 and $\text{Eu}_3\text{Ti}_2\text{O}_7$, the theoretical saturation magnetization values were calculated as $N_{\text{Eu}^{2+}} \times g\mu_B J$. These values are indicated by arrows in Fig. 4. The measured saturation magnetization values are in good quantitative agreement with these theoretical predictions, confirming the important role of Eu^{2+} ions in the magnetic properties of these materials.

The magnetic entropy change (ΔS_m) was evaluated from a series of the M - T curves according to the Maxwell relation

$$\Delta S_m(T, H) = \int_0^H \left(\frac{\partial M}{\partial T} \right)_H dH, \quad (2)$$

where H is the applied magnetic field. Figure 7 shows $-\Delta S_m$ of our composites. The $-\Delta S_m$ curve exhibits a characteristic caret-like shape, consistent with second order magnetic phase transitions.

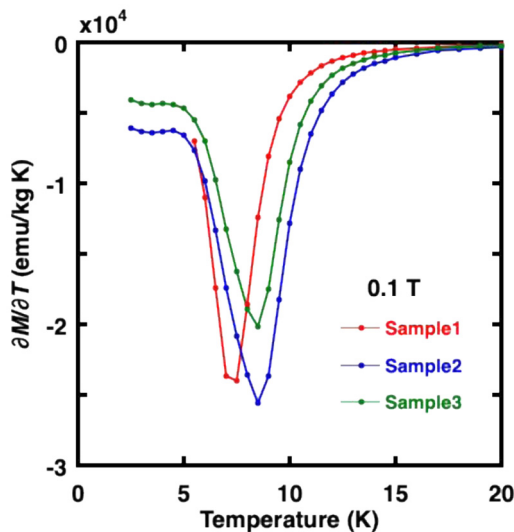


FIG. 5. Temperature derivative of magnetization $\frac{\partial M}{\partial T}$ as a function of temperature in 0.1 T for samples 1, 2, and 3.

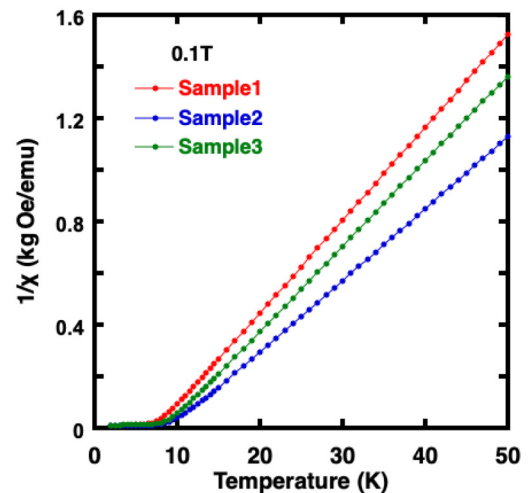


FIG. 6. Inverse magnetic susceptibility ($1/\chi$) as a function of temperature for samples 1, 2, and 3.

18 August 2025 09:55:45

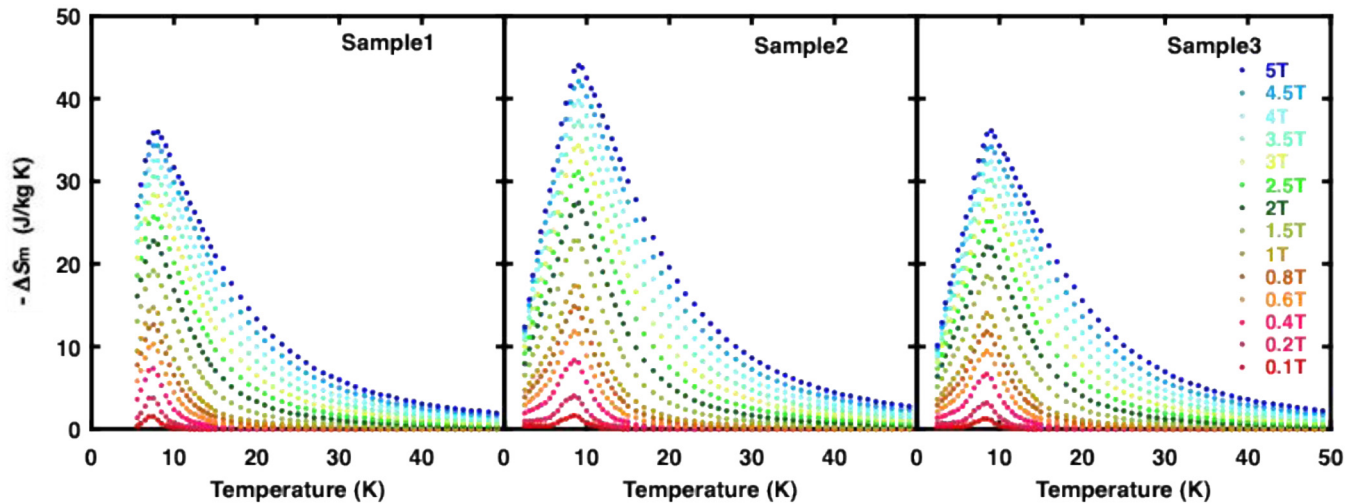


FIG. 7. Magnetic entropy change $-\Delta S_m$ as a function of temperature for the composite samples in various applied magnetic fields (0.1, 0.2, 0.4, 0.6, 0.8, 1, 1.5, 2, 2.5, 3, 3.5, 4, 4.5, and 5 T), calculated from magnetization data.

Figure 8 shows the $-\Delta S_m$ at 5 T for all three samples. $-\Delta S_m$ shows a peak near the respective T_c of each sample. The maximum $-\Delta S_m$ values of samples 1 and 3 are nearly identical, which is consistent with their similar total content of Eu_2TiO_4 and $\text{Eu}_3\text{Ti}_2\text{O}_7$. The peak temperature for sample 1 is lower than that of sample 3, reflecting the presence of $\text{Eu}_3\text{Ti}_2\text{O}_7$ in sample 1, which has a lower T_c . As observed in M , the magnitude of the $-\Delta S_m$ correlates with the amount of Eu_2O_3 . Sample 2 without Eu_2O_3 exhibits the largest $-\Delta S_m$, reaching a maximum value of 43.8 J/kg K. At the hydrogen liquefaction temperature 20.3 K, the $-\Delta S_m$ for sample 2 is still

significant value of 19.4 J/kg K. These results demonstrate that our composite materials exhibit giant MCE and are promising materials among oxide magnetic refrigerants. The data confirm that Eu_2TiO_4 and $\text{Eu}_3\text{Ti}_2\text{O}_7$ are responsible for the observed MCE and that minimizing Eu_2O_3 is crucial for maximizing performance. The difference in $-\Delta S_m$ between samples 1 and 3 in Fig. 8 suggests that Eu_2TiO_4 exhibits a greater entropy change at high temperatures compared to $\text{Eu}_3\text{Ti}_2\text{O}_7$, which is consistent with its higher T_c .

C. Entropy temperature diagram and adiabatic temperature change

Figure 9 shows the entropy-temperature diagram for composite sample 2, which exhibits the largest MCE among our composites. The entropy at various magnetic fields $S(T, H)$, was calculated by adding $\Delta S_m(T, H)$ (determined in Sec. III B) to the zero field entropy $S(T, 0)$ (from Sec. III A), using the relation $S(T, H) = S(T, 0) + \Delta S_m(T, H)$. An example of a Carnot cycle is shown as a solid rectangle. Further discussion follows in Secs. IV B and IV C.

The adiabatic demagnetization process can be evaluated using an entropy-temperature diagram. As illustrated in Fig. 9, during adiabatic demagnetization, the temperature of the material decreases from an initial temperature (T_i) to a final temperature (T_f) as the magnetic field is reduced from an initial field (H_i) of 5 T to zero. The T_f values obtained under various conditions are plotted on the left side of Fig. 10. The adiabatic temperature changes ($\Delta T_{ad} = T_i - T_f$) are shown on the right side of Fig. 10. ΔT_{ad} exhibits a peak value of 15.5 K when T_i is 25.5 K under a 5 T field, resulting in a final temperature of 10 K. A final temperature of 20 K can be achieved from a T_i of 29.5 K using a 5 T field. These results suggest that composite sample 2 has significant potential as a refrigerant material for hydrogen liquefaction and produces sub-cooled liquid hydrogen.

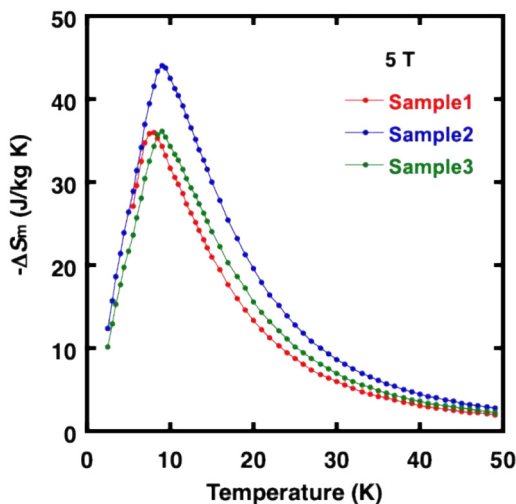


FIG. 8. Temperature dependence of $-\Delta S_m$ at 5 T for the composite samples.

18 August 2025 09:55:45

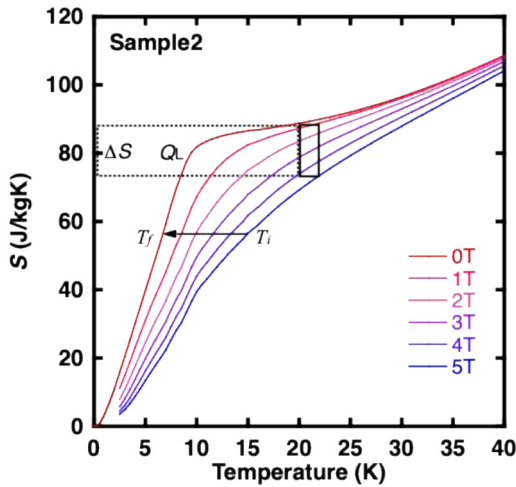


FIG. 9. Temperature dependence of entropy $S(T, H)$ of composite sample 2 in 0, 1, 2, 3, 4, and 5 T. The solid rectangle represents an example of the Carnot cycle operating between $T_L = 20$ K and $T_H = 22$ K. The area of the rectangle represented by the dashed lines corresponds to the amount of heat Q_L absorbed during the isothermal demagnetization process. The solid arrow represents an example of the adiabatic demagnetization process from $T_i = 15$ K and $H_i = 5$ T to T_f and 0 T.

It is important to note that evaluating entropy necessitates integrating specific heat and magnetization data, which inherently introduces some integration-related errors. In Sec. IV, we will compare the entropy of various materials. A certain degree of error is unavoidable because these calculations rely on entropy changes, specific heats, and other values derived from the existing literature.

IV. DISCUSSION

A. Comparison of magnetic entropy change with other oxide magnetic refrigerants

In this section, we compare the performance of our composite material with other oxide magnetic refrigerants such as garnets and

perovskites. Due to the limited available volume in high magnetic field applications, a comparison based on volumetric entropy change is particularly important. Figure 11 shows the temperature dependence of $-\Delta S_m$ at 5 T for several oxide materials: GGG,^{19,21,22} DGAG,^{9,19} GTP,²⁷ ETP,³⁴ GAP,^{28,29} and our composite sample 2. Our composite sample 2 exhibits the largest $-\Delta S_m$ in the temperature range from 7 to 26 K, demonstrating a significant advantage over these other oxide refrigerants. The maximum volumetric $-\Delta S_m$ achieved by sample 2 exceeds $0.3 \text{ J/cm}^3\text{K}$. It is worth noting that the bulk density was used to calculate the volumetric $-\Delta S_m$ for sample 2, reflecting its composite sintered nature. For the other materials, theoretical densities derived from their crystal structure were used.

Our composite sample 2 exhibits a significantly higher MCE than the garnet refrigerant GGG, which is a common benchmark material in cryogenic magnetic refrigeration applications. DGAG has also been used in experimental magnetic refrigerators for hydrogen liquefaction.^{9,10} Above 4 K, sample 2 outperforms both GGG and DGAG. At 20 K, a key temperature for hydrogen liquefaction, the $-\Delta S_m$ of sample 2 is about 3.7 times greater than that of GGG.

Perovskite oxides have been considered candidate refrigerants for hydrogen magnetic refrigeration due to their higher percentage of magnetic elements, potentially higher T_c compared to garnets, and chemical stability against hydrogenation. While GAP is an antiferromagnet whose MCE has been studied,^{28,29} our composite samples exhibit a significantly larger MCE than GAP over nearly the entire temperature range. ETP, which belongs to the same Eu-Ti-O system, exhibits an antiferromagnetic transition at 5.5 K. Our composites with Eu_2TiO_4 and $\text{Eu}_3\text{Ti}_2\text{O}_7$ exhibit much larger $-\Delta S_m$ than that of ETP³⁴ above the T_c of EuTiO_3 . In particular, the $-\Delta S_m$ of our sample 2 is approximately two times larger than that of ETP³⁴ at 20 K. This superior performance is attributed to the higher T_c and ferromagnetic interactions present in our composites. GTP, with a T_c (33 K) near the boiling point of hydrogen (20 K), was also studied for its MCE.²⁷ GTP undergoes a second order paramagnetic–ferrimagnetic transition involving Gd^{3+} and Ti^{3+} ions. As shown in Fig. 11, the $-\Delta S_m$ of GTP peaks at 33 K, but its value at 20 K is about half that of our sample 2. These comparisons clearly demonstrate the superior performance of our Eu_2TiO_4 and

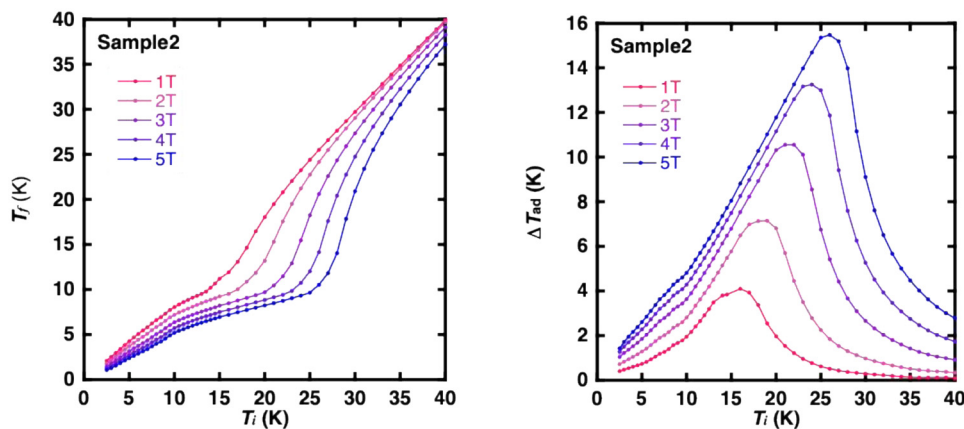


FIG. 10. (Left) T_f in adiabatic demagnetization process as functions of T_i from various H_i of 1, 2, 3, 4, and 5 T to zero. (Right) ΔT_{ad} as functions of T_i .

18 August 2025 09:55:45

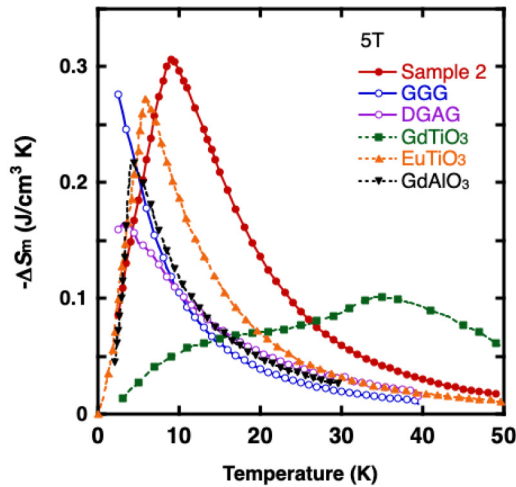


FIG. 11. Volumetric magnetic entropy change ($-\Delta S_m$) at 5 T for sample 2 compared with those of GGG, DGAG, GTP, ETP, and GAP.

$\text{Eu}_3\text{Ti}_2\text{O}_7$ composite compared to other oxide magnetic refrigerants. This superiority results from their relatively high T_c (close to 10 K) and the presence of ferromagnetic interactions.

The $-\Delta S_m$ of our sample 2 is comparable to that of GLF at 5 K and more than twice as large as that of GLF above 10 K.¹⁷ This suggests the potential for using our material in ADRs to extend their operating temperature range to higher temperatures, as will be discussed in Sec. IV C.

B. Cooling capacity in Carnot cycles for hydrogen liquefaction

A Carnot cycle is represented by a rectangle on an entropy-temperature diagram. As illustrated in Fig. 9, a Carnot cycle for hydrogen liquefaction between $T_L = 20$ K and $T_H = 22$ K is shown as a rectangle represented by solid lines. The area of the rectangle represented by the dashed lines corresponds to the amount of heat ($Q_L = T_L \times |\Delta S|$) absorbed during the isothermal demagnetization process.

The heat absorbed per unit volume by the magnetic refrigerant during a Carnot cycle was calculated from the entropy-temperature diagram for our composite sample 2 and several other oxide refrigerants (GGG, DGA, GTP, GAP, and ETP). Data were obtained from the literature and our own measurements for GGG,^{19,21,22} DGAG,^{9,19} GTP,²⁷ GAP,^{28,29} and ETP.³⁴ Two Carnot cycle scenarios were considered: one with a heat absorption temperature (T_L) of 20 K and a heat rejection temperature (T_H) of 22 K and the other with $T_L = 20$ K and $T_H = 25$ K. The resulting cooling capacities are compared in Fig. 12.

A comparison of the Q_L in Carnot cycles (Fig. 12) and the $-\Delta S_m$ (Fig. 11) highlights the crucial role of the temperature dependence of the zero-field entropy in achieving a wide temperature span and large cooling capacity. As shown in Fig. 9, the size of the Carnot cycle rectangle on the S - T diagram decreases significantly

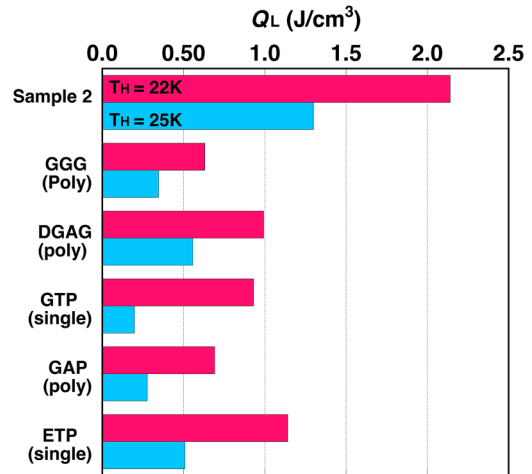


FIG. 12. Cooling capacity Q_L in a Carnot cycle for the composite sample 2 in comparison with GGG, DGAG, GTP, GAP, and ETP. Two cases were calculated: one with a heat absorbing temperature (T_L) of 20 K and a heat rejection temperature (T_H) of 22 K, and the other with $T_L = 20$ K and $T_H = 25$ K.

when the zero-field entropy increases rapidly due to lattice specific heat and/or Schottky specific heat from crystal field splitting, even though the $-\Delta S_m$ is large. GTP is an example in which the zero-field entropy plays an important role. Our composite sample 2 demonstrates approximately four times the cooling capacity of GGG. This superior performance highlights the advantage of magnetic refrigerants containing Eu_2TiO_4 and $\text{Eu}_3\text{Ti}_2\text{O}_7$ for Carnot cycle operation compared to other oxide magnetic refrigerants.

Recently, the use of subcooled liquid hydrogen has been proposed to reduce transfer loss of liquid hydrogen.⁵¹ In this concept, liquid hydrogen is cooled below 20 K. As shown in the S - T diagram (Fig. 9), our composite shows that the refrigeration capacity increases with decreasing operation temperature. The temperature dependence of refrigeration capacity will be discussed in Sec. IV C. In addition to chemical stability against hydrogen, our composite offers an advantage over metal-based magnetic refrigerants.

C. Characteristics of the composite material for the high temperature stage of adiabatic demagnetization refrigerator

The S - T diagram shown in Fig. 9 suggests that the temperature range with the highest refrigeration capacity for the composite material is close to the T_c . To evaluate the potential of our composite as a material suitable for the high temperature stage of ADR, we analyzed the temperature dependence of $-\Delta S$ obtained in a Carnot cycle. Figure 13 shows the volumetric $-\Delta S$ as a function of the heat absorption temperature (T_L). For comparison, data for standard materials such as GGG^{19,21,22} and GLF^{16,17} are also shown. Solid and dashed lines represent $-\Delta S$ values at 5 T calculated for Carnot cycles with temperature spans (ΔT) of 2 and 5 K, respectively.

Our composite material exhibits the largest $-\Delta S$ at temperatures slightly above T_c . GLF exhibits a significantly larger $-\Delta S$

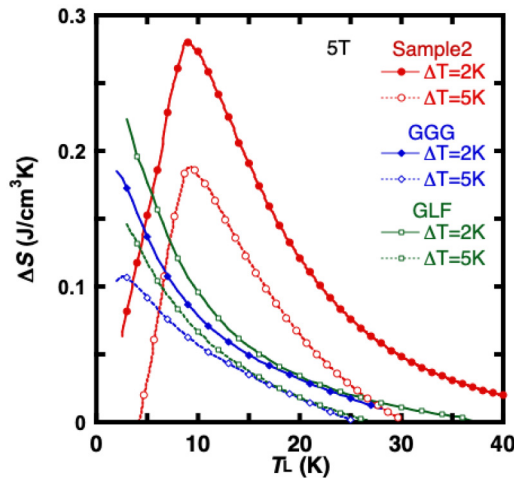


FIG. 13. Magnetic entropy changes in Carnot cycles with a temperature span of 2 and 5 K as functions of heat absorbing temperature (T_L) for the composite sample 2 in comparison with GGG and GLF. The applied magnetic field is 5 T. Solid and dashed lines show the cases of temperature span with 2 and 5 K, respectively.

compared to GGG at temperatures below about 10 K. The $-\Delta S$ of our composite material decreases below T_c . However, it remains larger than that of GLF and GGG at temperatures above about 5 K. This crossover temperature exhibits a slight variation with the applied magnetic field strength. These results indicate that the composite material is promising as a magnetic refrigerant for the high temperature stage of ADR, enabling an increase in the heat rejection temperature. Furthermore, as shown in Fig. 8, $-\Delta S$ tends to increase at lower temperatures with the increasing $\text{Eu}_3\text{Ti}_2\text{O}_7$ content. This suggests that the material properties can be tailored by adjusting the composition ratio.

Magnetic refrigeration systems typically use bulk materials in various shapes (plates, cylinders, and spheres). Ceramic materials offer the advantage of easy fabrication into various shapes, as demonstrated in previous studies.^{9–11,19} We have successfully synthesized ceramic samples of our composite material with a high relative density. This ease of processing makes the materials developed in this study particularly promising for practical applications.

While single-phase materials of Eu_2TiO_4 and $\text{Eu}_3\text{Ti}_2\text{O}_7$ were not synthesized in this study, the individual MCE contributions of each phase remain an open question. The magnitude of exchange interactions (both nearest neighbor and next nearest neighbor), crystal field effects, and lattice specific heat in each phase are different so that further investigations are needed to understand their MCE behavior in detail. This study has demonstrated that oxide ferromagnets containing Eu^{2+} ions exhibit large MCE in the cryogenic temperature range and are promising magnetic refrigerants.

V. CONCLUSIONS

This study investigated the MCE in magnetic oxides containing Eu_2TiO_4 and $\text{Eu}_3\text{Ti}_2\text{O}_7$, focusing on the large magnetic

moment of Eu^{2+} ions. Specific heat measurements revealed distinct peaks at 8 and 7 K, corresponding to the transition temperatures of Eu_2TiO_4 and $\text{Eu}_3\text{Ti}_2\text{O}_7$, respectively. The relative peak magnitudes were consistent with the $\text{Eu}_2\text{TiO}_4/\text{Eu}_3\text{Ti}_2\text{O}_7$ ratios in the samples. The observed magnetic entropy release was in good agreement with the theoretical value for Eu^{2+} ion in a $J = 7/2$ free spin state and no magnetic moment of Ti^{4+} ions. Similarly, the saturation magnetization was in agreement with the expected value for Eu^{2+} ions and Ti^{4+} ions. The maximum volumetric magnetic entropy change of our composite exceeded $0.3 \text{ J/cm}^3\text{K}$, which is significantly higher than that of established oxide magnetic refrigerants. The entropy change of our composite was about 3.7 times larger than that of GGG at the hydrogen liquefaction temperature of 20 K. The specific heat and magnetization results were combined to obtain an entropy–temperature diagram. Analysis of the entropy–temperature diagram revealed that our material exhibits a cooling capacity several times higher than that of other oxide refrigerants (GGG, DGAG, GTP, GAP, and ETP) when implemented in a hydrogen liquefaction Carnot cycle. Our composite materials also show potential for extending the operating temperature range of ADRs to higher temperatures.

ACKNOWLEDGMENTS

This work was supported by the JST-Mirai Program under Grant No. JPMJMI18A3, Japan. The authors appreciate Dr. Hiroya Sakurai for useful discussions.

AUTHOR DECLARATIONS

Conflict of Interest

The authors have no conflicts to disclose.

Author Contributions

Koichi Matsumoto: Conceptualization (lead); Funding acquisition (lead); Investigation (lead); Methodology (lead); Project administration (lead); Supervision (lead); Visualization (lead); Writing – original draft (lead); Writing – review & editing (lead). **Masaki Horie:** Formal analysis (equal); Investigation (equal). **Hironori Hasegawa:** Formal analysis (equal); Investigation (equal). **Kazuhiro Ishikawa:** Investigation (equal). **Shuhei Yamazaki:** Investigation (equal). **Hideaki Kitazawa:** Investigation (equal); Methodology (equal); Resources (equal); Writing – review & editing (equal). **Akiko T. Saito:** Investigation (equal); Methodology (equal); Writing – review & editing (equal). **Takenori Numazawa:** Project administration (equal); Resources (equal).

DATA AVAILABILITY

The datasets generated and/or analyzed during the current study are available from the corresponding author upon reasonable request.

REFERENCES

- ¹P. Debye, “Einige Bemerkungen zur Magnetisierung bei tiefer Temperatur,” *Ann. Phys.* **386**(25), 1154–1160 (1926).

- ²W. F. Giaque, "Paramagnetism and the third law of thermo-dynamics. Interpretation of the low-temperature magnetic susceptibility of gadolinium sulfate," *J. Am. Chem. Soc.* **49**(8), 1870–1877 (1927).
- ³K. A. Gschneidner Jr, V. K. Pecharsky, and A. O. Tsokol, "Recent developments in magnetocaloric materials," *Rep. Prog. Phys.* **68**(6), 1479–1539 (2005).
- ⁴A. Kitanovski, J. Tušek, U. Tomc, U. Plaznik, M. Ožbolt, and A. Poredoš, *Magnetocaloric Energy Conversion* (Springer International Publishing, Cham, 2015).
- ⁵J. Lyubina, "Magnetocaloric materials for energy efficient cooling," *J. Phys. D Appl. Phys.* **50**(5), 053002 (2017).
- ⁶V. Franco, J. S. Blázquez, J. J. Ipus, J. Y. Law, L. M. Moreno-Ramírez, and A. Conde, "Magnetocaloric effect: From materials research to refrigeration devices," *Prog. Mater. Sci.* **93**, 112–232 (2018).
- ⁷S. Sherif, N. Zeytinoglu, and T. Veziroglu, "Liquid hydrogen: Potential, problems, and a proposed research program," *Int. J. Hydrogen Energy* **22**(7), 683–688 (1997).
- ⁸A. T. Wijayanta, T. Oda, C. W. Purnomo, T. Kashiwagi, and M. Aziz, "Liquid hydrogen, methylcyclohexane, and ammonia as potential hydrogen storage: Comparison review," *Int. J. Hydrogen Energy* **44**(29), 15026–15044 (2019).
- ⁹T. Numazawa, K. Kamiya, T. Utaki, and K. Matsumoto, "Magnetic refrigerator for hydrogen liquefaction," *Cryogenics (Guildf.)* **62**, 185–192 (2014).
- ¹⁰T. Numazawa, K. Kamiya, S. Yoshioka, H. Nakagome, K. Matsumoto, J. G. Weisend, J. Barclay, S. Breon, J. Demko, M. DiPirro, J. P. Kelley, P. Kittel, A. Klebaner, A. Zeller, M. Zagarola, S. Van Sciver, A. Rowe, J. Pfotenhauer, T. Peterson, and J. Lok, "Development of a magnetic refrigerator for hydrogen liquefaction," *AIP Conf. Proc.* **985**, 1183–1189 (2008).
- ¹¹K. Matsumoto, T. Kondo, S. Yoshioka, K. Kamiya, and T. Numazawa, "Magnetic refrigerator for hydrogen liquefaction," *J. Phys. Conf. Ser.* **150**(1), 012028 (2009).
- ¹²K. Ohira, K. Nakamichi, and H. Furumoto, "Experimental study on magnetic refrigeration for the liquefaction of hydrogen," *Adv. Cryog. Eng.* **45**, 1747–1754 (2000).
- ¹³K. Kamiya, K. Matsumoto, T. Numazawa, S. Masuyama, H. Takeya, A. T. Saito, N. Kumazawa, K. Futatsuka, K. Matsunaga, T. Shirai, S. Takada, and T. Iida, "Active magnetic regenerative refrigeration using superconducting solenoid for hydrogen liquefaction," *Appl. Phys. Express* **15**(5), 053001 (2022).
- ¹⁴P. J. Shirron, E. R. Canavan, M. J. DiPirro, J. G. Tuttle, and C. J. Yeager, "A multi-stage continuous-duty adiabatic demagnetization refrigerator," *Adv. Cryog. Eng.* **45**, 1629–1638 (2000).
- ¹⁵J. Tuttle, E. Canavan, H. Delee, M. DiPirro, A. Jahromi, B. James, M. Kimball, P. Shirron, D. Sullivan, and E. Switzer, "Development of a space-flight ADR providing continuous cooling at 50 mK with heat rejection at 10 K," *IOP Conf. Ser. Mater. Sci. Eng.* **278**, 012009 (2017).
- ¹⁶M. DiPirro, E. Canavan, P. Shirron, and J. Tuttle, "Continuous cooling from 10 to 4 K using a toroidal ADR," *Cryogenics (Guildf.)* **44**(6–8), 559–564 (2004).
- ¹⁷T. Numazawa, K. Kamiya, P. Shirron, M. DiPirro, and K. Matsumoto, "Magnetocaloric effect of polycrystal GdLiF₄ for adiabatic magnetic refrigeration," *AIP Conf. Proc.* **850**, 1579–1580 (2006).
- ¹⁸K. A. Gschneidner and V. K. Pecharsky, "Magnetocaloric materials," *Annu. Rev. Mater. Sci.* **30**(1), 387–429 (2000).
- ¹⁹P. Wikus, E. Canavan, S. T. Heine, K. Matsumoto, and T. Numazawa, "Magnetocaloric materials and the optimization of cooling power density," *Cryogenics (Guildf.)* **62**, 150–162 (2014).
- ²⁰J. A. Barclay and W. A. Steyert, "Materials for magnetic refrigeration between 2 K and 20 K," *Cryogenics (Guildf.)* **22**(2), 73–80 (1982).
- ²¹T. Numazawa, H. Kimura, M. Sato, and H. Maeda, "Carnot magnetic refrigerator operating between 1.4 and 10 K," *Cryogenics (Guildf.)* **33**(5), 547–554 (1993).
- ²²Y. Hakuraku and H. Ogata, "A magnetic refrigerator for superfluid helium equipped with a rotating superconducting magnet system," *Jpn. J. Appl. Phys.* **25**(1R), 140 (1986).
- ²³R. A. Fisher, G. E. Brodale, E. W. Hornung, and W. F. Giaque, "Magnetothermodynamics of gadolinium gallium garnet. I. Heat capacity, entropy, magnetic moment from 0.5 to 4.2 °K, with fields to 90 kG along the [100] axis," *J. Chem. Phys.* **59**(9), 4652–4663 (1973).
- ²⁴P. Schiffer, A. P. Ramirez, D. A. Huse, and A. J. Valentino, "Investigation of the field induced antiferromagnetic phase transition in the frustrated magnet: Gadolinium gallium garnet," *Phys. Rev. Lett.* **73**(18), 2500–2503 (1994).
- ²⁵R. D. McMichael, J. J. Ritter, and R. D. Shull, "Enhanced magnetocaloric effect in Gd₃Ga_{5-x}Fe_xO₁₂," *J. Appl. Phys.* **73**(10), 6946–6948 (1993).
- ²⁶K. Matsumoto, A. Matsuzaki, K. Kamiya, and T. Numazawa, "Magnetocaloric effect, specific heat, and entropy of iron-substituted gadolinium gallium garnets Gd₃(Ga_{1-x}Fe_x)₅O₁₂," *Jpn. J. Appl. Phys.* **48**(11), 113002 (2009).
- ²⁷H. Omote, S. Watanabe, K. Matsumoto, I. Gilmudtinov, A. Kiamov, and D. Tayurskii, "Magnetocaloric effect in single crystal GdTlO₃," *Cryogenics (Guildf.)* **101**, 58–62 (2019).
- ²⁸T. King, B. A. Ramirez, P. J. Shirron, E. R. Canavan, M. J. DiPirro, J. S. Panek, J. G. Tuttle, R. D. Shull, and R. A. Fry, "Rare-earth garnets and perovskites for space-based ADR cooling at high T and low H," *AIP Conf. Proc.* **613**, 1191–1200 (2002).
- ²⁹M. D. Kuz'min and A. M. Tishin, "Magnetic refrigerants for the 4.2–20 K region: Garnets or perovskites?," *J. Phys. D Appl. Phys.* **24**(11), 2039–2044 (1991).
- ³⁰Y. Su, Y. Sui, X. Wang, J. Cheng, Y. Wang, W. Liu, and X. Liu, "Large magnetocaloric properties in single-crystal dysprosium titanate," *Mater. Lett.* **72**, 15–17 (2012).
- ³¹Y. Su, Y. Sui, J. Cheng, X. Wang, Y. Wang, W. Liu, and X. Liu, "Large reversible magnetocaloric effect in HoTiO₃ single crystal," *J. Appl. Phys.* **110**(8), 083912 (2011).
- ³²Y. Su, Y. Sui, J. Cheng, X. Wang, Y. Wang, P. Liu, and J. Tang, "Large reversible magnetocaloric effect in TmTiO₃ single crystal," *J. Appl. Phys.* **111**(7), 07A925 (2012).
- ³³Z.-J. Mo, J. Shen, L. Li, Y. Liu, C.-C. Tang, F.-X. Hu, J.-R. Sun, and B.-G. Shen, "Observation of giant magnetocaloric effect in EuTiO₃," *Mater. Lett.* **158**, 282–284 (2015).
- ³⁴A. Midya, P. Mandal, K. Rubi, R. Chen, J. S. Wang, R. Mahendiran, G. Lorusso, and M. Evangelisti, "Large adiabatic temperature and magnetic entropy changes in EuTiO₃," *Phys. Rev. B* **93**(9), 094422 (2016).
- ³⁵B. T. Matthias, R. M. Bozorth, and J. H. Van Vleck, "Ferromagnetic interaction in EuO," *Phys. Rev. Lett.* **7**(5), 160–161 (1961).
- ³⁶K. Ahn, A. O. Pecharsky, K. A. Gschneidner, and V. K. Pecharsky, "Preparation, heat capacity, magnetic properties, and the magnetocaloric effect of EuO," *J. Appl. Phys.* **97**(6), 063901 (2005).
- ³⁷K. Matsumoto, L. Li, S. Hirai, E. Nakamura, D. Murayama, Y. Ura, and S. Abe, "Large magnetocaloric effect in sintered ferromagnetic EuS," *Cryogenics (Guildf.)* **79**, 45–48 (2016).
- ³⁸D. X. Li, T. Yamamura, S. Nimori, Y. Homma, F. Honda, Y. Haga, and D. Aoki, "Large reversible magnetocaloric effect in ferromagnetic semiconductor EuS," *Solid State Commun.* **193**, 6–10 (2014).
- ³⁹G. J. McCarthy, W. B. White, and R. Roy, "The system Eu-Ti-O: Phase relations in a portion of the 1400 °C isotherm," *J. Inorg. Nucl. Chem.* **31**(2), 329–339 (1969).
- ⁴⁰C.-L. Chien, S. DeBenedetti, and F. D. S. Barros, "Magnetic properties of EuTiO₃, Eu₂TiO₄, and Eu₃Ti₂O₇," *Phys. Rev. B* **10**(9), 3913–3922 (1974).
- ⁴¹T. Katsufuji and H. Takagi, "Coupling between magnetism and dielectric properties in quantum paraelectric EuTiO₃," *Phys. Rev. B* **64**(5), 054415 (2001).
- ⁴²V. Scagnoli, M. Alliet, H. Walker, M. Scavini, T. Katsufuji, L. Sagarna, O. Zaharko, and C. Mazzoli, "EuTiO₃ magnetic structure studied by neutron powder diffraction and resonant x-ray scattering," *Phys. Rev. B* **86**(9), 094432 (2012).
- ⁴³A. P. Petrović, Y. Kato, S. S. Sunku, T. Ito, P. Sengupta, L. Spalek, M. Shimuta, T. Katsufuji, C. D. Batista, S. S. Saxena, and C. Panagopoulos, "Electric field modulation of the tetragonal domain orientation revealed in the magnetic ground state of quantum paraelectric EuTiO₃," *Phys. Rev. B* **87**(6), 064103 (2013).
- ⁴⁴S. N. Ruddlesden and P. Popper, "New compounds of the K₂NiF₄ type," *Acta Crystallogr.* **10**(8), 538–539 (1957).
- ⁴⁵S. N. Ruddlesden and P. Popper, "The compound Sr₃Ti₂O₇ and its structure," *Acta Crystallogr.* **11**(1), 54–55 (1958).

- ⁴⁶J. E. Greedan and G. J. McCarthy, "Crystal chemistry and magnetic properties of Eu_2TiO_4 and $\text{Eu}_3\text{Ti}_2\text{O}_7$," *Mater. Res. Bull.* **7**(6), 531–541 (1972).
- ⁴⁷C.-L. Chien, S. DeBenedetti, and F. D. Barros, "Ferrimagnetic properties of $\text{Eu}_3\text{Ti}_2\text{O}_7$," *Phys. Lett. A* **44**(3), 178–180 (1973).
- ⁴⁸K. Momma and F. Izumi, "VESTA 3 for three-dimensional visualization of crystal, volumetric and morphology data," *J. Appl. Crystallogr.* **44**(6), 1272–1276 (2011).
- ⁴⁹N. L. Huang and J. H. Van Vleck, "Effect of the anisotropic exchange and the crystalline field on the magnetic susceptibility of Eu_2O_3 ," *J. Appl. Phys.* **40**(3), 1144–1146 (1969).
- ⁵⁰A. M. Lejus and J. C. Bernier, "Proprietes magnetiques de l'oxyde Eu_2O_3 monocristallin," *Mater. Res. Bull.* **11**(5), 477–482 (1976).
- ⁵¹D. Truck, "Linde link for truck refueling using liquid hydrogen," *Fuel Cells Bull.* **2021**(1), 3–4.